

Ce³⁺ doped CeP₂O₇ Ceramic Electrolyte for high temperature Proton Exchange Membrane Fuel Cell

Xin Huang¹, Gang Wang², Min Huang¹, Yuming Deng¹, MingMing Fei¹, Chenxi Xu^{1,*}, Jigui Cheng^{1,*}

¹ School of Materials Science and Engineering, Hefei University of Technology, Hefei, Anhui, China

² China quality certification centre, Beijing, China, 100070

*E-mail: xuchenxi31@126.com, jgcheng63@sina.com

Received: 10 January 2017 / Accepted: 9 February 2017 / Published: 12 March 2017

Proton conductors capable of operating in high temperature range (over 180oC) has attracted worldwide attention. The promising inorganic membranes candidates CeP₂O₇ and Ce³⁺ doped CeP₂O₇ were used between 160 °C and 280 °C for Proton exchange membrane fuel cell (PEMFC) in this study. The structure and phase stability were analyzed by X-ray diffraction, Fourier transform infrared (FTIR), XPS (ESCALAB250Xi) and thermogravimetric analysis (TGA), and also the microstructure morphology was analyzed by scanning electron microscopy (SEM). The CeP₂O₇ and Ce³⁺ doped CeP₂O₇ composite membranes exhibited high proton conductivity of 0.008 S cm⁻¹ and 0.0095S cm⁻¹ at 200 °C, respectively. The peak power densities of Ce³⁺ doped CeP₂O₇ membrane were 23.5 mW cm⁻² at 180 °C and 26.6 mW cm⁻² at 200 °C, respectively.

Keywords: high-temperature proton exchange membrane fuel cells; low valency cations; cerium pyrophosphate

1. INTRODUCTION

During the years, proton exchange membrane fuel cells (PEMFC) at high temperature as electrochemical have attracted much attention. Operating a PEMFC at elevated temperatures could provide many advantages such as 1) lower Pt loading requirements or making it possible to use non-noble metal catalyst 2) improved CO tolerances leading to simplified fuel pre-treatment techniques, and, 3) improving the efficiency of the fuel cell [1-4]. Research on proton exchange membranes for medium temperature (120-180°C) operating under low humidity is usually focused on polybenzimidazole based membranes. PBI is typically doped with phosphoric acid (PA) to provide proton conductivity [2, 6]. PBI/PA membrane has good conductivity and acceptable mechanical strength and impermeability for PEMFC. However, the limitations of liquid PA, such as its

deactivation via phosphate anion adsorption at positive potentials, acid leaching, and degradation to pyrophosphate at temperatures over 160°C, restrict PBI/PA used in a higher temperature ranges [6-8].

Recently, a number of tetravalent metal pyrophosphates (MP_2O_7 , where $M = Sn, Ge, Zr, Si, Ce, Ti$) have shown significant proton conductivity ($\sim 10^{-2} \text{ S cm}^{-1}$) [9-12]. Therefore, many efforts have been made to develop these kinds of materials. Hibino et al. [11] reported that the proton conductivities of SnP_2O_7 materials high conductivity via doping with trivalent elements. Wang et al. reported that the fuel cell using $Sn_{0.9}In_{0.1}P_2O_7$ as an electrolyte yields power densities of 14.7 mW cm^{-2} under H_2/O_2 conditions at 443K, respectively. In the literature works, Cerium pyrophosphate has suitable protonic conductivity in 150–250°C range [14-18]. Song et al. researched Gd^{3+} Doped Cerium Pyrophosphate, which exhibited a conductivity of $2.91 \times 10^{-2} \text{ S cm}^{-1}$ at 190°C [14]. The low proton conductivity is still the main problem for the metal pyrophosphate materials as the electrolyte. Doping with low valence cation ($Al^{3+}, In^{3+}, Mg^{2+}, Ga^{3+}, Sc^{3+}, Mg^{2+}$ etc) [11] in MP_2O_7 materials by partial substitution of M^{4+} is an usually potential way to improve the conductivity because of charge compensation for the low valency cations that provide more number of jump sites and facilitates the hopping of protons. However, doping the low valence cation are normally the different elements, this may affect the structure uniform and even thermal degradation.

In this study, we promoted 10% Ce^{3+} -doped cerium pyrophosphate ($Ce^{4+}P_2O_7$) as the crystalline phase to achieve a single structure formation. The doping of lower valence cations into CeP_2O_7 could provide more oxygen vacancies in the materials and would increase the basicity of the material bulk [19-20]. The 10% Ce^{3+} doped CeP_2O_7 membrane proton conductivity was and fuel cell performance range from 180-250°C were studied, and the results indicated that the performance of the inorganic composite membrane was suitable for HT-PEMFC.

2. EXPERIMENTAL

Ce^{3+} doped CeP_2O_7 was prepared as follows. Briefly CeO_2 and $CeCl_3$ powder were mixed in stoichiometric proportions (9:1) and ball-milled for 8 h at 300 rpm using zirconia balls in isopropyl alcohol and then dried at 70 °C for about 20 h. The dried CeO_2 - $CeCl_3$ particles were mixed with 85% H_3PO_4 . This mixture was held with stirring at 90 °C until a high viscosity paste achieved. The paste was calcined in an alumina pot at 350 °C for 2.5 h in N_2 gas ambience to prevent Ce^{3+} oxidized to completely Ce^{4+} . The calcined powder was pressed into pellet disks under 200 MPa. The disks (13-mm diameter) were sintered at 300 °C for 8 h in a closed alumina crucible at N_2 protection and were polished with sandpaper. The thickness of the pellet membrane is 1mm. A CeP_2O_7 powder was also prepared using commercially CeO_2 particle.

The membrane was painted with colloidal silver on both sides, and dried in an oven at 120°C for 2 hrs. The proton conductivity was measured by the two-point probe method with an AutolabPGSTAT302. The impedance measurements were carried out between frequencies of 1 and 10 kHz. The perturbation voltage was kept at 10mV. The crystal structures of different powders were analysed by X-ray diffraction (XRD, X'Pert PROMPD), with scan range of 5–80° over 2 hrs. The morphologies of the membrane were investigated by a SU-8020 Scanning Electron Microscope.

Fourier transform infrared spectroscopy (FTIR) of different samples was measured on Nicolet 67FT-IR spectrometer system between 4000 and 300 cm^{-1} . The thermal behaviour was analysed by Thermogravimetric Analysis (TGA, STA449F3). XPS measurement was carried on out on a spectrometer (ESCALAB250Xi) with a Ka anticathode.

Catalyst inks were prepared by blending carbon-supported catalysts (40 wt. % Pt/C, Alfa Aesar) in a water–ethanol mixture under ultrasonic vibration for 30 mins [21, 22]. The ink was deposited on membrane for both anode and cathode directly, and then the MEA were held at 150 °C for 2 hrs. The Pt loading achieves 0.2 mg cm^{-2} . The silver wires were connected to the sample by the conductive adhesive. 5vol% H_2/Ar and air were fed into anode and cathode at flow rates of 50 $\text{cm}^3 \text{min}^{-1}$ and atmospheric pressure, respectively.

3. RESULTS AND DISCUSSION

Figure 1 shows the powder XRD pattern confirming diffraction peaks of CeP_2O_7 (JCPDS 16-0584). The (111), (200), (210), (211), (311), (222), (400), (311), (420), (333), (422), (511), (440), (531) and (600) crystal planes of CeP_2O_7 were corresponded to the XRD angles at 17.83° , 20.71° , 22.19° , 25.45° , 27.63° , 35.80° , 37.11° , 42.57° , 46.81° , 47.92° , 52.36° , 56.87° , 62.78° , 64.74° and 65.93° that follows literatures reported [9]. The incorporation of Ce^{3+} into the CeP_2O_7 lattice occur because the effective ionic radius of trivalent Ce^{3+} is same to Ce^{4+} (0.087 nm). The lattice parameters calculated form XRD is $C=8.52 \text{ \AA}$ which fits well agreed with the standard pattern data.

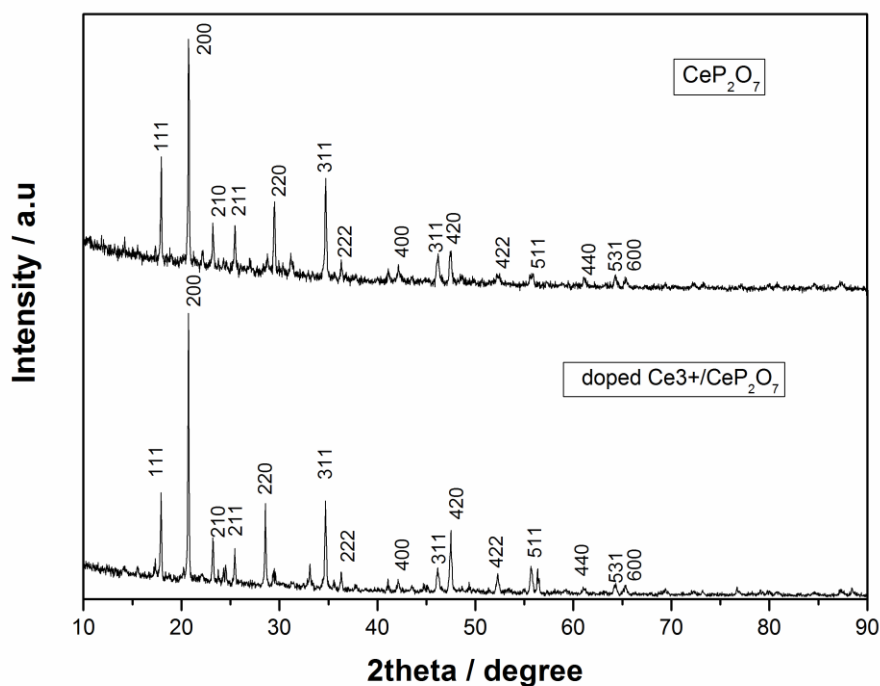


Figure 1. XRD pattern of CeP_2O_7 and CeP_2O_7 with Cu K X-rays

SEM images (Fig. 2) depict the cross section morphologies of CeP_2O_7 and Ce^{3+} doped CeP_2O_7 sintered pellets. In Fig. 2a, it is observed that The pellets are not completely dense, and the presence of micrometer-size pores can be seen. Fig.2b shows that Ce^{3+} -doped CeP_2O_7 particles are mostly cubic shape and size homogeneously. The particle size of Ce^{3+} -doped CeP_2O_7 seems larger than the CeP_2O_7 that may result a decrease proton transmit due to the small contact area between crystal grains. The densities of the CeP_2O_7 and Ce^{3+} -doped CeP_2O_7 pellet calculated by Archimedes' method, were 2.09 g cm^{-3} and 2.98 g cm^{-3} , respectively. This density result indicates that the less pores in the Ce^{3+} -doped CeP_2O_7 membrane that benefits to inhibit the gas crossover.

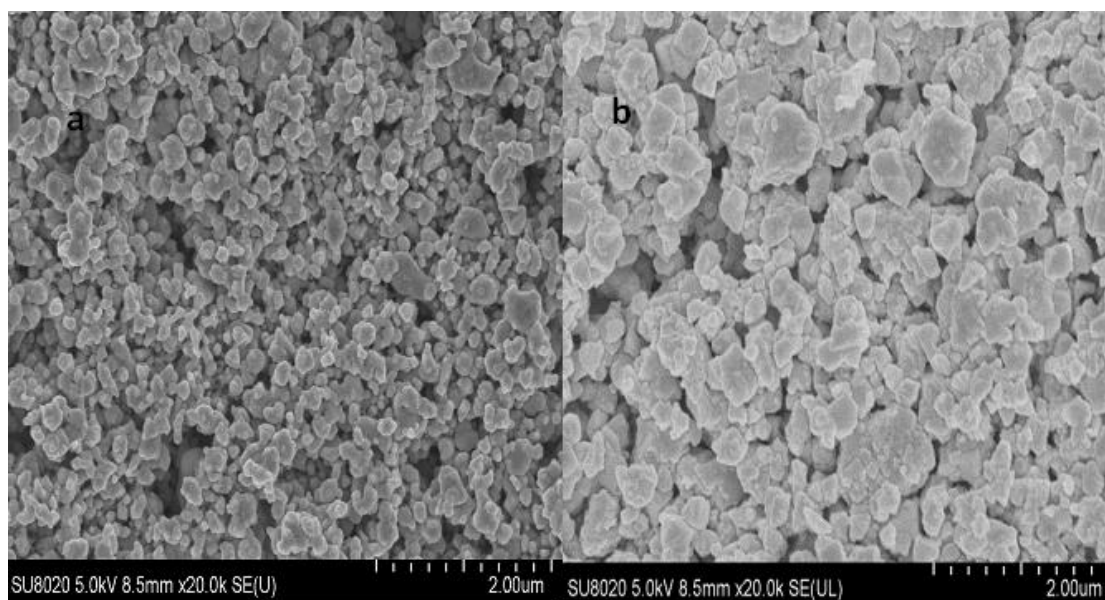


Figure 2. SEM images of membrane cross-sections: a) CeP_2O_7 and b) Ce^{3+} doped CeP_2O_7

FTIR studies on CeP_2O_7 and Ce^{3+} -doped CeP_2O_7 are shown in Fig. 3. The appearance of the broad band at 1290 cm^{-1} can be assigned to the P-O-H in plane bending vibration of CeP_2O_7 . The symmetric and asymmetric stretching frequencies of PO_3 in $\text{P}_2\text{O}_7^{4-}$ are observed at 1090 and 1210 cm^{-1} , respectively. The asymmetric and symmetric P-O-P bridge stretching modes are generally observed in the regions $970\text{--}930 \text{ cm}^{-1}$ (960 cm^{-1}) and $780\text{--}740 \text{ cm}^{-1}$ (747 cm^{-1}) regions [23-27]. There was no significant difference between two curves indicating the same chemical element in the materials.

As Fig.4 depicted, the coexistence of the Ce^{3+} and Ce^{4+} oxidation states are distinguishable [28]. The Ce (3d3/2) and Ce (3d5/2) XPS spectrum obtained from the fine particles are shown in Fig. 4. In addition, Ce^{4+} binding energy peaks at 885.1eV , 898.5eV , 915.5eV , and also two peaks corresponding to Ce^{3+} species at 881.7eV and 903.1eV on the Ce^{3+} doped CeP_2O_7 were clearly observed. The spectral shape shows the existence of two oxidation states Ce^{3+} and Ce^{4+} , which confirmed the successful doping of Ce^{3+} in the $\text{Ce}^{4+}\text{P}_2\text{O}_7$.

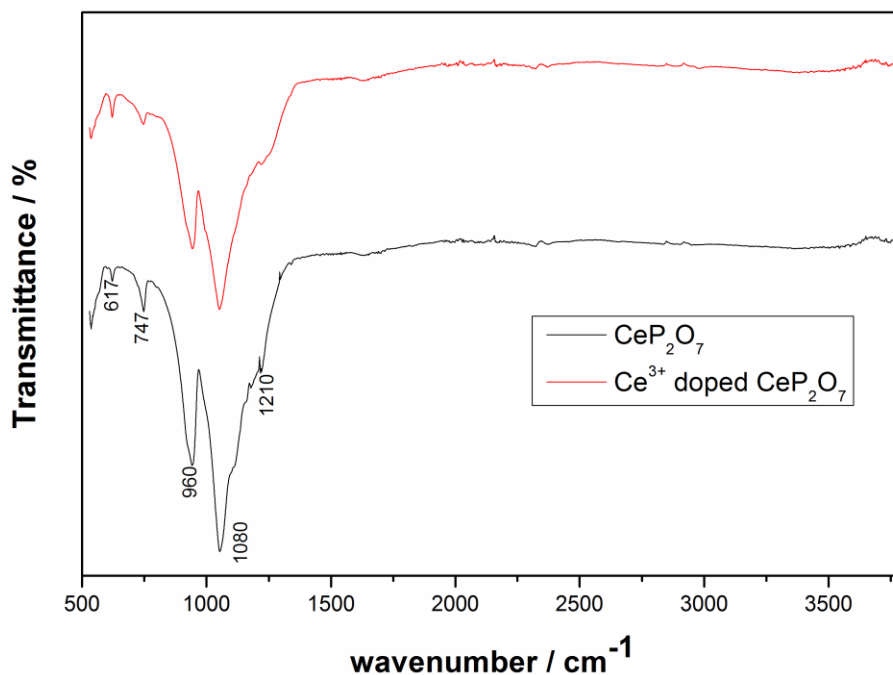


Figure 3. Infrared spectra of CeP_2O_7 and Ce^{3+} -doped CeP_2O_7 with the test resolution of 4 cm^{-1}

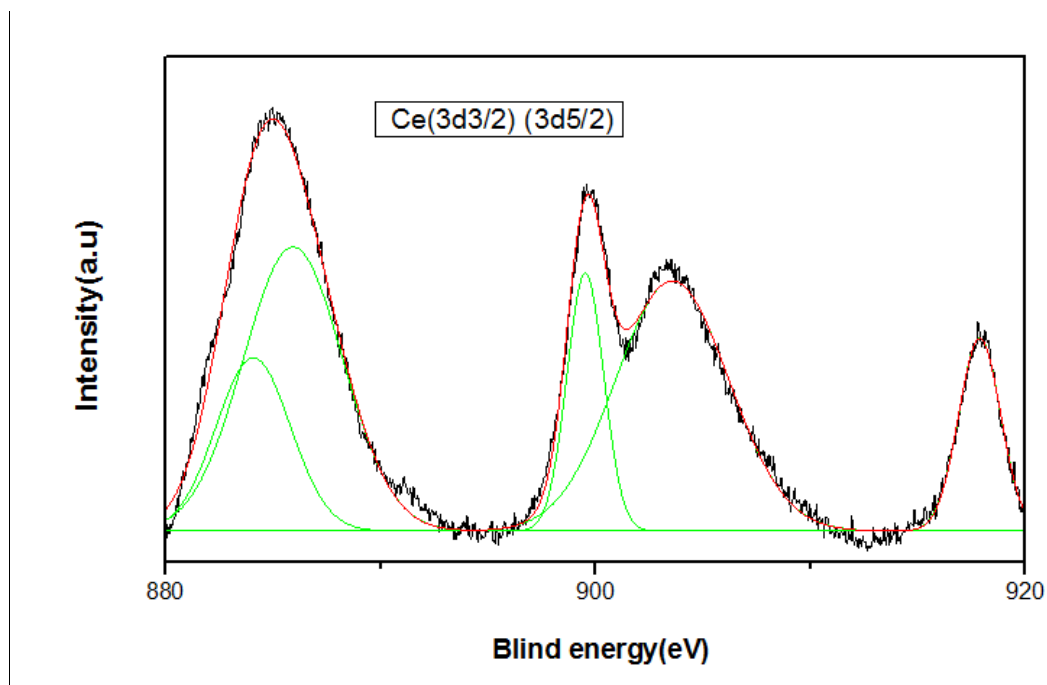


Figure 4. XPS Ce 3d photoemission spectra for Ce (3d3/2) and Ce (3d5/2)

The thermal stability of the CeP_2O_7 and Ce^{3+} doped CeP_2O_7 membranes is studied range from room temperature to $800\text{ }^\circ\text{C}$ shown in Fig. 5. There are three prominent regions of CeP_2O_7 weight loss in the TGA curve. The initial weight loss of about 2.5% below $180\text{ }^\circ\text{C}$ in region 1 is caused by the water loss. The second region is mainly attributed to the partial thermal decomposition of CeP_2O_7 into CePO_4 , CeP_3O_9 , CeO_2 and $\text{Ce}(\text{PO}_4)_3$ [23]. The third decrease part as shown in region 3 is appearance

of a prominent endotherm at 500°C, which is caused by the decomposition of cerium pyrophosphate into phosphate, metaphosphate and polyphosphate [30]. It was obviously seen that the Ce³⁺ doped CeP₂O₇ keeping stable until 800 °C. The presence of Ce³⁺ ions is in favour of the existence of stronger hydrogen bond between the Ce-O networks [31] or weaker intermolecular forces between the P-O-P bonds [32] that may explain the reason for the stability of Ce³⁺ doped CeP₂O₇.

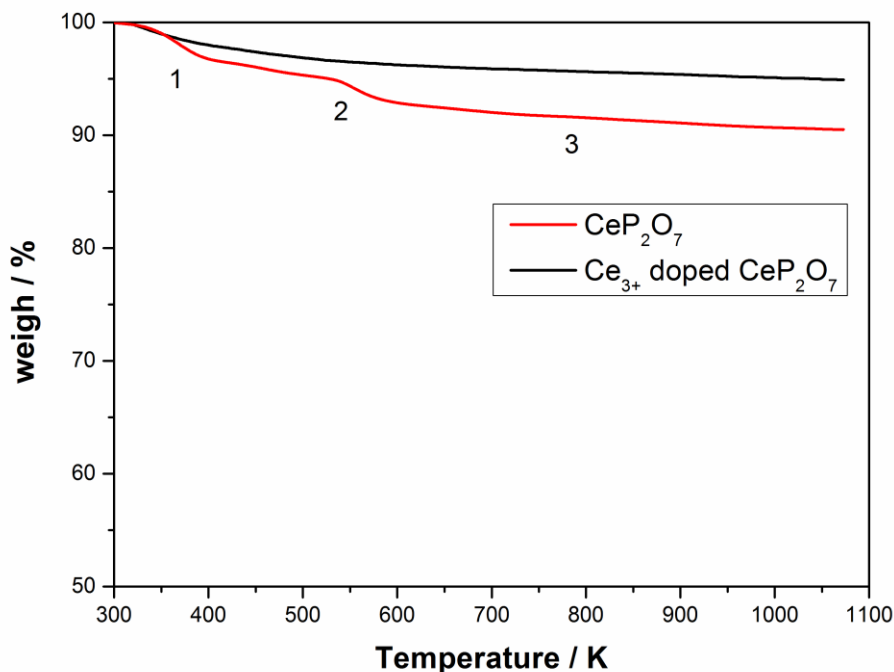


Figure 5. TGA of the prepared CeP₂O₇, Ce³⁺ doped CeP₂O₇ heated from room temperature to 800 °C with a heating rate of 5 °C min⁻¹

The conductivity of the CeP₂O₇ membranes is calculated from the impedance data at 150–280°C. CeP₂O₇ exhibits a measurable conductivity at range of 5.8×10⁻³ S cm⁻¹ to 8.3×10⁻³ S cm⁻¹ from 160°C to 200°C in non-humid atmosphere, and then the conductivity decreases to 2.9×10⁻³ S cm⁻¹ while the temperature up to 280°C in Fig. 6. The conductivity is assumed that a partial disconnection of the P₂O₇ network for proton conduction caused by the phosphate deficiency that follows the Grotthuss mechanism [34]. The protonic conduction of the solid membrane is incorporated into the CeP₂O₇ bulk by the following reactions. [11]



Where O_o^\bullet , V_o^x , OH_o^x , PO_4 and HP_2O_7 denote a lattice oxide ion, an oxygen vacancy, an interstitial proton, phosphate ions and hydrogen pyrophosphate defects at pyrophosphate sites, respectively.

The curve in Fig. 6 clearly illustrates that the Ce³⁺ doped CeP₂O₇ (0.01 S cm⁻¹ at 200 °C) has a higher conductivity by contrast the CeP₂O₇ membrane in the temperature of 150-280°C. In addition to, the CeP₂O₇ structure includes a network of MO₆ octahedra sharing corners with P₂O₇ units,

characterized by the presence of intersecting zigzag tunnels delimited by pentagonal windows [32-34]. This specific structure could provide several ion exchange sites and transport pathways which performance as the proton conductivity. Typically, the low valency cations are introduced into the bulk of CeP_2O_7 by the partial substitution of Ce^{4+} cations is a suitable way to improve the proton exchange capability [38]. The substitution of Ce^{3+} for Ce^{4+} -site increases the concentration of mobile charge carriers which is expected to increase the conductivity. [34]. The long-range mobility of the proton is much greater than that of the oxygen ion and electron hole [21, 33]. The higher proton conductivity of Ce^{3+} doped CeP_2O_7 is because of the presence of oxygen vacancies or holes, and also the formation of these charge carriers can be expressed, which benefits of the phosphate ions transmit. The pore size of the Ce^{3+} doped CeP_2O_7 membrane is larger than the non-doped membrane as shown in SEM image, that resulting in a reduced effective electric circuit of the membrane due to the small contact area between crystal grains. This may be the other reason to affect the conductivity results which should be further explored in the next work. However, in the temperature over 200°C conductivity began to reduce rapidly, which could be attributed to the decomposition of CeP_2O_7 , which could be attributed to the decomposition of CeP_2O_7 into secondary phosphate phases, as evidenced from the TGA data. These secondary phosphates such as CeO_2 , P_2O_5 , cerium orthophosphate (CePO_4) and cerium polyphosphates ($\text{Ce}_3(\text{PO}_4)_3$) [17-18] exhibit much lower ionic conductivity than that of CeP_2O_7 .

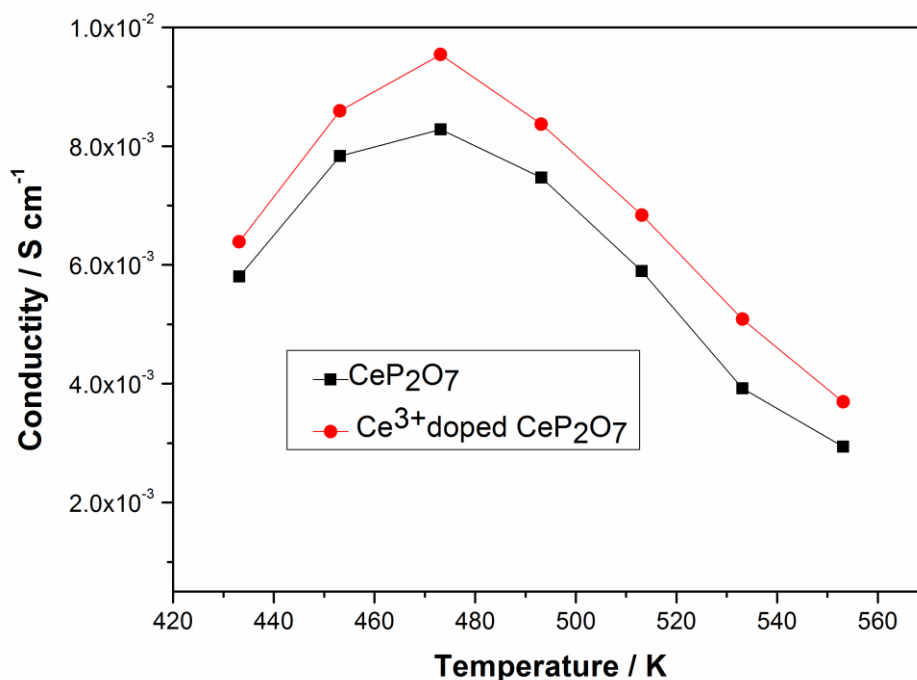


Figure 6. Conductivities of CeP_2O_7 and Ce^{3+} doped CeP_2O_7 composite membranes under anhydrous conditions.

As shown in Fig.7, the polarization and power density curves are obtained at 180°C and 200°C under dry conditions for CeP_2O_7 and Ce^{3+} doped CeP_2O_7 . The open circuit voltages (OCVs) of CeP_2O_7 and Ce^{3+} -doped CeP_2O_7 membranes are over 0.8V. The performances of the cells with the

Ce³⁺-doped CeP₂O₇ composite membranes are significantly better than that of the pristine CeP₂O₇ membrane. As Fig. 7 shown, the maximum power density of CeP₂O₇ was approximately 18 mW cm⁻² at the temperature of 200 °C , and the power density value of Ce³⁺ doped CeP₂O₇ was enhanced to 26.6 mW cm⁻². This improved performance is mainly caused by the superior proton conductivity because of the much proton hopping vacancies construction while Ce³⁺ doped. The power density of CeP₂O₇ incersed from 14.2 to 18.4 mWcm⁻² by increasing the temperature range from 180 to 200°C. The results were also accordance to the variation tendency of membranes conductivity. The voltage losses of the Ce³⁺-doped CeP₂O₇ membrane are 0.6 V and 0.3 V and the current losses of it from 0.033 to 0.08A cm⁻² at 200°C, and the result cell conductivities are approximately 0.0015 S cm⁻¹, which is smaller than the value from the conductivity test. Because, the potential drop of the fuel cell attributed to including the ohmic loss and the cathodic polarization loss [5, 30]. The thickness of membranes reduction and the density of membranes enhancement including electrode optimization should be the other suitable ways to improve the fuel cell performance.

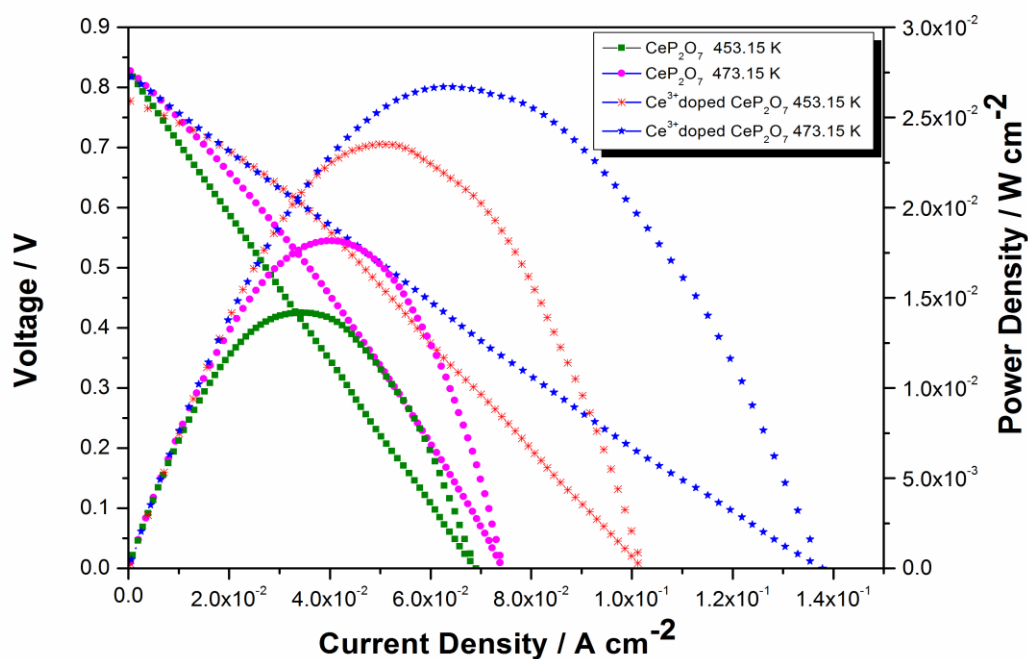


Figure 7. Polarization and power density curves of fuel cells operated at 180 °C and 200°C with 5vol% H₂/Ar and air at atmospheric pressure. Pt Loading is 0.2 mg cm⁻² both anode and cathode.

4. CONCLUSION

In this work, inorganic composite CeP₂O₇ and Ce³⁺ doped CeP₂O₇ electrolytes were synthetic completely. The doping of Ce³⁺ in CeP₂O₇ composite membranes leads to an increase in conductivity ranging from 0.006 to 0.01 S cm⁻¹ at temperatures ranging from 160 to 200 °C, although the membrane conductivity rapidly decreased when the temperature is more than 200°C. The Ce³⁺ doped

CeP₂O₇ membrane also suggested better performance results (with a peak power density: 26.2 mW cm⁻² at 200 °C) compared with the 14.2 mW cm⁻² result of the un-doped CeP₂O₇ membrane. These results conditionally suggest that this material is a potential candidate material for high temperature fuel cells.

ACKNOWLEDGMENTS

The authors thank the funding support provided by the National Natural Science Foundation of China (21606064) and the Anhui Provincial Natural Science Foundation (1508085QB45). This project was also supported by the 56th China Postdoctoral Science Foundation funded project, No. 2014M560506.

References

1. Y. Shao, G. Yinb, Z. Wang, Y. Gao. *J. Power. Sour.*, 167(2007) 235.
2. C. Xu, X. Wu, X. Wang, M. Mamlouk, K. Scott, *J. Mater. Chem.*, 34(2011) 6014.
3. QF. Li, JO. Jensen, RF. Savinell, Bjerrum, *Prog. Polym.Sci.*, 34(2009) 449.
4. J. Lobato, P. Canizares, MA. Rodrigo, JJ. Linares, JA. Aguilar, *J. Membr. Sci.*, 306(2007) 47.
5. T. Authayanun, M. Mamlouk, A. Arpornwichanop, *Int J Hydrogen Energy.*, 37(2012) 6808.
6. M. Mamlouk, K. Scott, *J. Power. Sour.*, 196(2011) 1084.
7. C. Xu, Y. Cao, R. Kumar, X. Wu, X. Wang, K. Scott, *J. Mater. Chem.*, 21(2011) 11359.
8. V. Nalini, MH. Sorby, K. Amezawa, R. Haugsrud, H. Fjellvag, T. Norby, *J. Am Ceram. Soc.*, 94(2011) 1514.
9. B. Singh, HN. Im, JY. Park, SJ. Song, *J. Phys. Chem C.*, 117(2013) 2653.
10. A. Tomita, N. Kajiyama, T. Kamiya, M. Nagao, T. Hibino, *J. Electrochem Soc.*, 154(2007) B1265.
11. Y. Sato, Y. Shen, M. Nishida, W. Kanematsub, T. Hibino, *J. Mater. Chem.*, 22(2012) 3973.
12. X. Huang, YM. Deng, C. Xu, Y. Hu, L. Yang, PY. Luo, W. Lu, *Fule.*, 179(2016) 299.
13. H. Wang, J. Chen, C. Luo, R. Qiao. *Solid. State Ionics.*, 263(2014) 71.
14. B. Singh, JH. Kim, O. Parkash, SJ. Song, *J. Electrochem. Soc.*, 162(2014) 464.
15. B. Singh, JH. Kim, O. Parkash, SJ. Song, *Ceramics International.*, 42(2016) 2983.
16. B. Singh, SY. Jeon, HN. Im, JY. Park, SJ. Song, *J. Alloys. Compd.* 578(2013) 279.
17. SJ. Onoda, Y. Inagaki, A. Kuwabara, N. Kitamura, K. Amezawa, Nakahira, I. Anaka, *J. Ceram. Process Res.*, 11(2010) 344.
18. VIL. Botto, EJ. Baran, *Z. Anorg. Allg. Chem.*, 430(1977) 283.
19. K. Genzaki, P. Heo, M. Sano, T. Hibino, *J. Electrochem. Soc.*, 156(2009) B806.
20. T. Nagao, A. Takeuchi, P. Heo, T. Hibino, M. Sano, A. Tomitab, *Electrochem. Solid. St.*, 9(2006) A105.
21. DR. Mullins, SH. Overbury DR. Hunntley, *Surf. Sci.*, 409(1998) 307.
22. JP. Holgado, G. Muneura, JP. Espinos, AR. Gonzalez-Elipse. *Appl. Surf. Sci.*, 158(2000) 164.
23. XF. Sun, SR. Wang, ZR. Wang, XF. Ye, Tl. Wen, F.Q. Huang, *Solid. State. Ionics.*, 179(2008) 1138.
24. A. Baykal, M. Kizilyalli, M. Toprak, R. Kniep, *Turk J. Chem.*, 25(2001) 425.
25. SD. Mikhailenko, J. Zaidi, S. Kaliaguine, *Trans. Faraday, Chem. J. Soc.*, 94(1998) 1613.
26. Z. Tao, W. Zhang, Y. Huang, D. Wei, H. Seo, *Solid. State. Sci.*, 34(2014) 78.
27. H. Wang, J. Liu, W. Wang, Ma. Guilin, *J. Power. Sour.*, 195(2010) 5596.
28. E. Beche, P. Charvin, D. Perarnau, S. Abanades, G. Flamant, *Surf. Interface Anal.*, 40(2008) 264.
29. B. Singh, SY. Jeon, JH. Kim, JY. Park, C. Bae, SJ. Song, *J. Electrochem Soc.*, 161(2014) 464.
30. A. Tomita, N. Kajiyama, T. Kamiya, M. Nagao, T. Hibino, *J. Electrochem. Soc.* 154(2007) 1256.
31. VP. Dotsenko, IV. Berezozskaya, NP. Efryushina, AS. Voloshinovskii, P. Dorenbos, CWE. Van

Eijk. *J. Lumin* (2001) 137.

32. Y. Ma, J. Wainright, M. Litt, R. Savinell, *J. Electrochem. Soc.*, 51(2004) 8.

33. O. Paschos, J. Kunze, U. Stimming, F. Maglia, *Matter.*, 23(2011) 234110.

34. T. Hibino, K. Kobayashi, *J.Mater. Chem.*, 1(2013) 1134.

© 2017 The Authors. Published by ESG (www.electrochemsci.org). This article is an open access article distributed under the terms and conditions of the Creative Commons Attribution license (<http://creativecommons.org/licenses/by/4.0/>).